THE JOURNAL OF PHYSICAL CHEMISTRY B
A JOURNAL OF THE AMERICAN CHEMICAL SOCIETY

pubs.acs.org/JPCB

Article

High-Speed Stimulated Raman Scattering Microscopy Using Inertia-Free AOD Scanning

Published as part of The Journal of Physical Chemistry virtual special issue "Xiaoliang Sunney Xie Festschrift".

Shuai Yan, Yiran Li, Zhiliang Huang, Xiaocong Yuan,* and Ping Wang*

Cite This: *J. Phys. Chem. B* 2023, 127, 4229–4234

Read Online

ACCESS | Metrics & More | Article Recommendations | Supporting Information

ABSTRACT: High-throughput stimulated Raman scattering (SRS) microscopy is highly desired for large tissue imaging with chemical specificity. However, the mapping speed remains as the major short board of conventional SRS, primarily owing to the mechanical inertia existing in galvanometers or other laser scanning alternatives. Here, we developed inertia-free acousto-optic deflector (AOD)-based high-speed large-field stimulated Raman scattering microscopy, in which both the speed and integration time are ensured by immune of the mechanical response time. To avoid laser beam distortion induced by the intrinsic spatial dispersion of AODs, two spectral compression systems are implemented to compress the broad-band femtosecond pulse to picosecond laser. We achieved an SRS imaging of a 12 × 8 mm^2 mouse brain slice in only 8 min at an image resolution of approximately 1 μm and 32 slices from a whole brain in 12 h. The AOD-based inertia-free SRS mapping can be much faster after further upgrading and allow broad-spectrum applications of chemical imaging in the future.

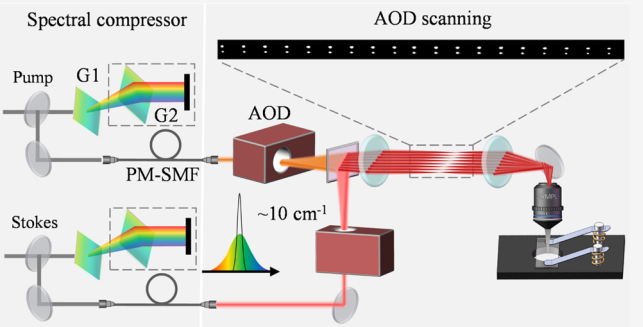

INTRODUCTION

Among the most advanced label-free microscopic imaging modalities, including second harmonic generation (SHG),[1−3] third harmonic generation (THG),[4] optical coherence tomography (OCT),[5,6] photoacoustic microscopy (PAM),[7] and other imaging methodologies,[8] stimulated Raman scattering (SRS) microscopy is distinct and recognized to be chemically and analytically advantageous by providing deterministic contrasts of various important small biomolecules marked with their intrinsic fingerprints in Raman spectra.[9−11] Over the last decade, SRS microscopy has made significant progresses in pushing the limits of sensitivity,[12,13] speed,[14,15] spatial resolution, and other key imaging performances.[16] These advances enabled numerous vital applications, including the chemical imaging of lipids and cholesterol in living cells,[17] tracking metabolic activities of glucose in brain and various organs,[18] characterizing arteriosclerosis in blood vessels or other diseased human tissues,[19] intraoperative pathology for identification of tumor,[20−22] and so on. However, in most cases, SRS microscopy was limited to either a very small field of view (FOV) about 300 μm or mapping a relatively large tissue in an insufferable long time.[23−25] In a recent advance, the microscopic SRS imaging time of a 12 × 7 mm^2 mouse brain section has been reduced from conventional 70 min to only 8 min.[26,27] However, to pursue the ultimate laser scanning speed, the pixel dwell time in this work was reduced to 2 μs, which almost reached the response limit of galvanometers. The resonant galvanometer and polygon scanner allowed video-rate imaging and rapid spectral scanning.[12,28,29] However, the mechanical inertia of the fast-moving mirrors is problematic, resulting in extremely short exposure time (~0.1 μs) and some extent of image distortion. Conversely, the polygon scanner takes advantage of the inertia of rotating heavy mass to maintain a constant scanning rate. However, the rotating speed often fluctuates and the scanning jitters occur from time to time. In addition, the field of view is difficult to be tuned for various imaging requirements.[30] Besides fundamental research, rapid and large-scale SRS mapping still remains as a standing challenge for developing fast label-free bedside pathology and other clinical applications.

Herein, we present high-speed large-scale SRS mapping enabled by a combination of acousto-optic deflector (AOD)-based inertia-free laser scanning and motorized stage, in which both the speed and integration time are ensured by immune of the scanner's response time. The deflection angle of the incident laser can be scanned by the radio frequencies fed into the AODs. Especially, two spectral compression systems are implemented

Received: December 30, 2022
Revised: April 21, 2023
Published: May 4, 2023

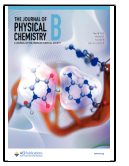

https://doi.org/10.1021/acs.jpcb.2c09114
J. Phys. Chem. B 2023, 127, 4229−4234

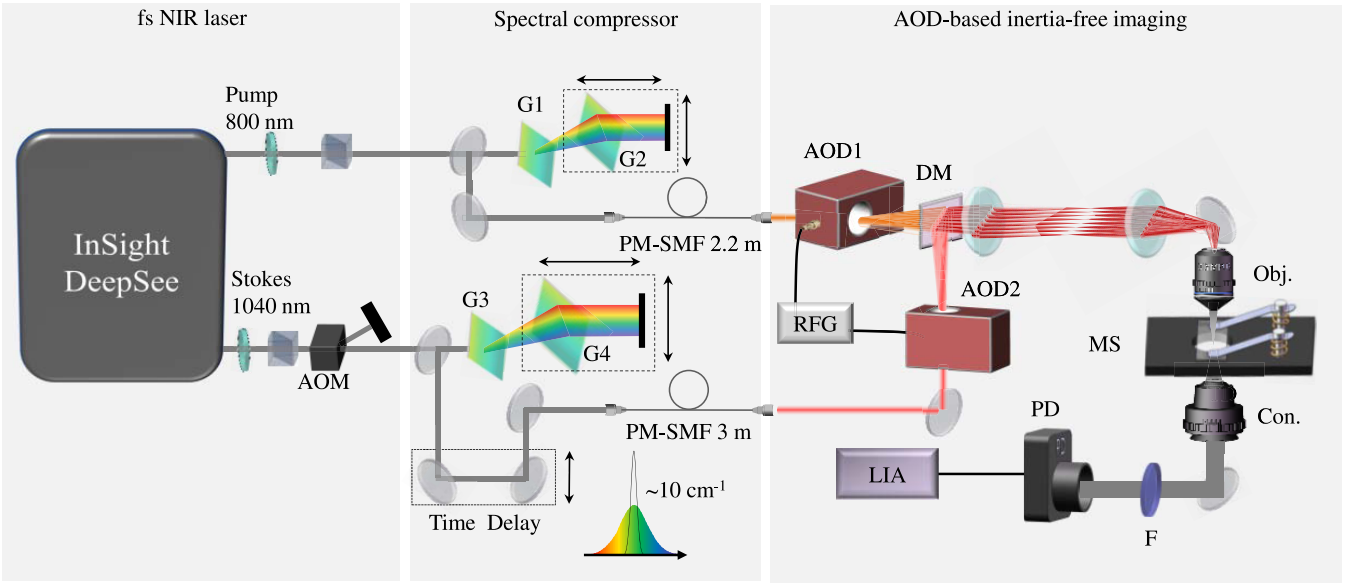

Figure 1. Schematic diagram of the AOD-based inertia-free high-speed stimulated Raman scattering microscopy. AOM: acousto-optic modulator, G: grating, PM-SMF: polarization-maintaining single-mode fiber, RFG: radio frequency generator, AOD: acousto-optic deflector, DM: dichroic mirror, Obj.: objective, MS: motorized stage, Con.: condenser, F: filter, PD: photodiode, LIA: lock-in amplifier.

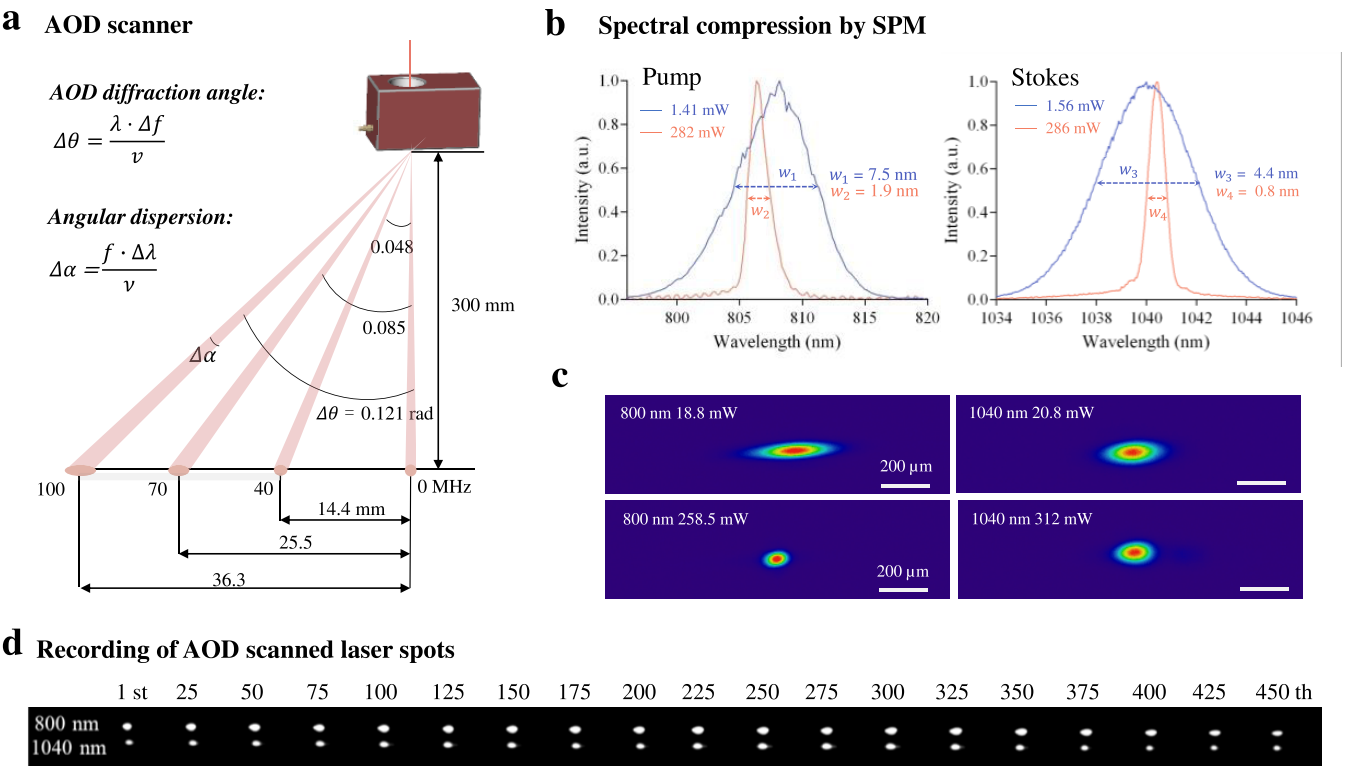

Figure 2. AOD diffraction and spectral compressing. (a) AOD scanning at various input RF frequencies. (b) Measurements of spectral width before and after spectral compression. (c) Focused beam shapes of AOD-diffracted first-order lasers before and after spectral compression. (d) Position matching of AOD-scanned laser spots.

to convert fs laser to narrow-band ps laser and meanwhile compensate AOD-induced beam dispersion.[31] With a 0.9 NA 40× objective (UPLSAPO, Olympus), we successfully demonstrated SRS mapping of intact mouse brain section (12 × 8 mm^2) in only 8 min at an image resolution of approximately 1 μm and a dwell time of 4 μs and 32 slices of a whole brain in 12 h. Furthermore, the FOV and imaging speed can be substantially improved by applying a high NA 25× objective. The AOD-based inertia-free laser scanning method will make up the current short board of SRS and allow a broad spectrum of molecular imaging applications in the future.

EXPERIMENTAL METHODS

AOD-Based High-Speed Large-Field SRS Microscopy. Both pump and Stokes beams are provided by a femtosecond laser (InSight DeepSee, Spectra-Physics, Newport) with a

https://doi.org/10.1021/acs.jpcb.2c09114
J. Phys. Chem. B 2023, 127, 4229−4234

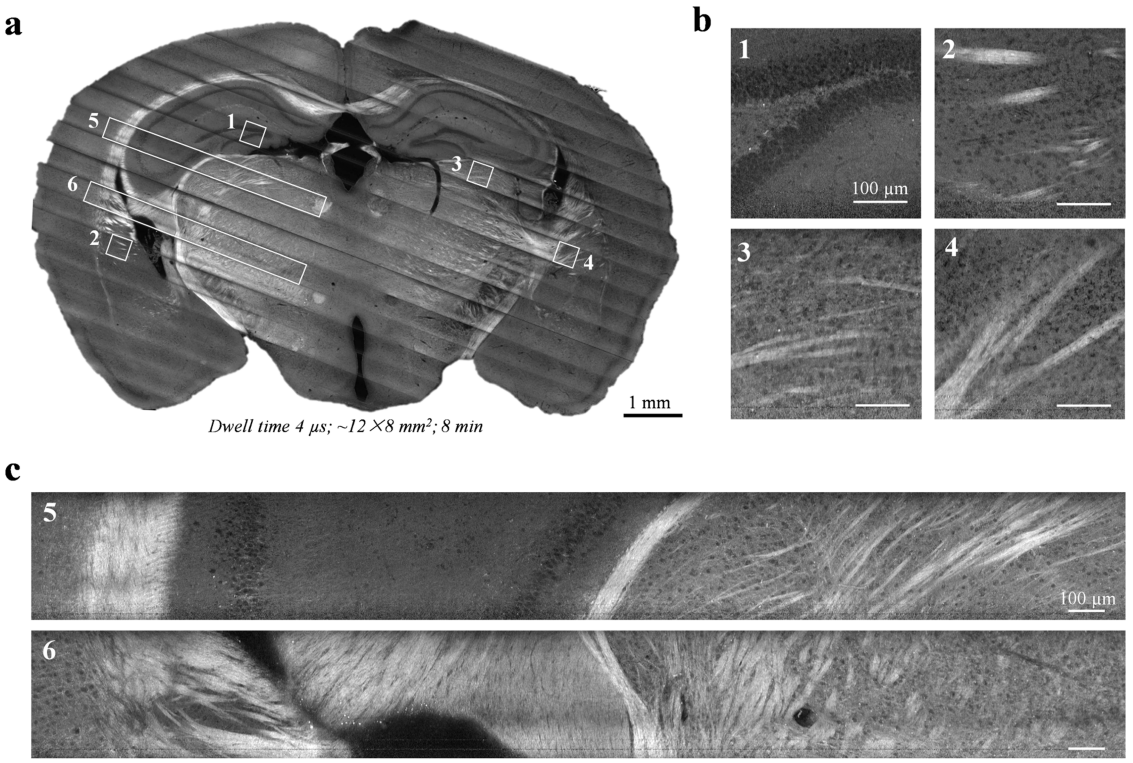

Figure 3. High-speed SRS mapping of intact mouse brain section. (a) SRS image of a 12 × 8 mm^2 brain section. Scale bar, 1 mm. (b, c) Zoom-in images at locations of 1−6 in panel (a). Scale bar, 100 μm.

repetition rate of 80 MHz (Figure 1). To match the carbon−hydrogen (CH) vibrations of biological systems, the wavelengths of pump and Stokes lasers were set at 800 nm (~100 fs) and 1040 nm (~200 fs), respectively. The Stokes laser was further modulated in intensity by an acousto-optic modulator (AOM) at 2.5 MHz for further lock-in detection. Both pump and Stokes lasers entered independent spectral compressors to convert fs laser to narrow-band ps laser. Two AODs, driven by an arbitrary waveform generator (DG4162, RIGOL) and two power amplifiers (ZHL-1-2W-S, Mini-Circuits), were utilized to scan the pump and Stokes lasers (Figure 2a). They were spatially combined by a dichroic mirror (DMSP1000, Thorlabs) and then delivered to a 40× objective through an achromatic lens set (AC508-400-B and AC508-200-B). A motorized stage was synchronized with AOD scanners to fulfill a relatively large tissue imaging. The transmitted lasers from the sample were collected by a condenser, and the pump beam was optically filtered by two short-pass filters (ET980sp, Chroma) and detected by a photodiode. The SRS signal was extracted by a resonant amplifier and a lock-in amplifier at 2.5 MHz.

Spectral Compressor. To compress the spectral width of a broad-band fs laser, a pair of gratings were employed to introduce negative chirping. For the 1040 nm Stokes laser, the transmission of the double-pass grating pair is approximately 80% because the diffraction efficiency of the grating is as high as 95%. Furthermore, a polarization-maintaining single-mode fiber (PM-SMF) compressed the spectral width of the Stokes laser by self-phase modulation (SPM). The optimized coupling efficiency of PM-SMF was measured to be about 50%. Thus, the overall transmission of our spectral compression system for Stokes laser was roughly 40%, corresponding to 60% in power loss. For the pump laser, the overall power loss was slightly higher (70%). For the pump beam, two gratings were spaced at a distance of 4 cm, and a 2.2 m long PM-SMF (PM780-HP, Nufern) was adopted after the grating pair (1200 l/mm @840 nm, Wasatch Photonics). As the results shown in Figures 2b and S1, the spectral width was compressed at the most by a factor of ~3.9 with a laser power of 282 mW in PM-SMF, corresponding to a spectral width reduction from 7.5 to 1.9 nm in full width at half-maximum (FWHM). The pulse duration of the pump laser was broadened to 2.35 ps in FWHM (Figure S2). For the Stokes beam, we adjusted the grating separation (1000 l/mm, LSFSG-1000, Lightsmyth) to 9 cm and delivered 286 mW laser into a 3 m PM-SMF (PM980-XP, Nufern) to achieve the best spectral compression. The original spectral width of the Stokes laser, 4.4 nm in FWHM, was successfully compressed 5.5 times to 0.8 nm, and the pulse duration was broadened to 3.6 ps.

The spectral width of the pump laser in Figure 2b was measured by a spectrometer (USB2000, Ocean Optics) with a wavelength range of 200−1025 nm. The spectral width of the Stokes laser (1040 nm) was evaluated by a home-built spectrometer consisting of a holographic grating (1200 l/mm, Wasatch Photonics), an achromatic doublet lens (AC508-150-B, Thorlabs), and an NIR CCD camera. The different wavelengths of the laser were dispersed and focused on the Fourier plane of the lens and then imaged by the camera. The measurements of the pulse width in Figure S2 were performed by an autocorrelator (Carpe, APE). To evaluate the beam quality after AOD and the performance of the spectral compressor (Figure 2c), an NIR camera was allocated to the focal position of a 400 mm AC lens.

Laser Settings and Data Acquisition. For brain slice imaging, the laser powers of pump and Stokes beams were 40 and 200 mW, respectively. The input frequencies of the AODs were set at 47.38−85.69 MHz for pump and 39.06−68.38 MHz

https://doi.org/10.1021/acs.jpcb.2c09114
J. Phys. Chem. B 2023, 127, 4229−4234

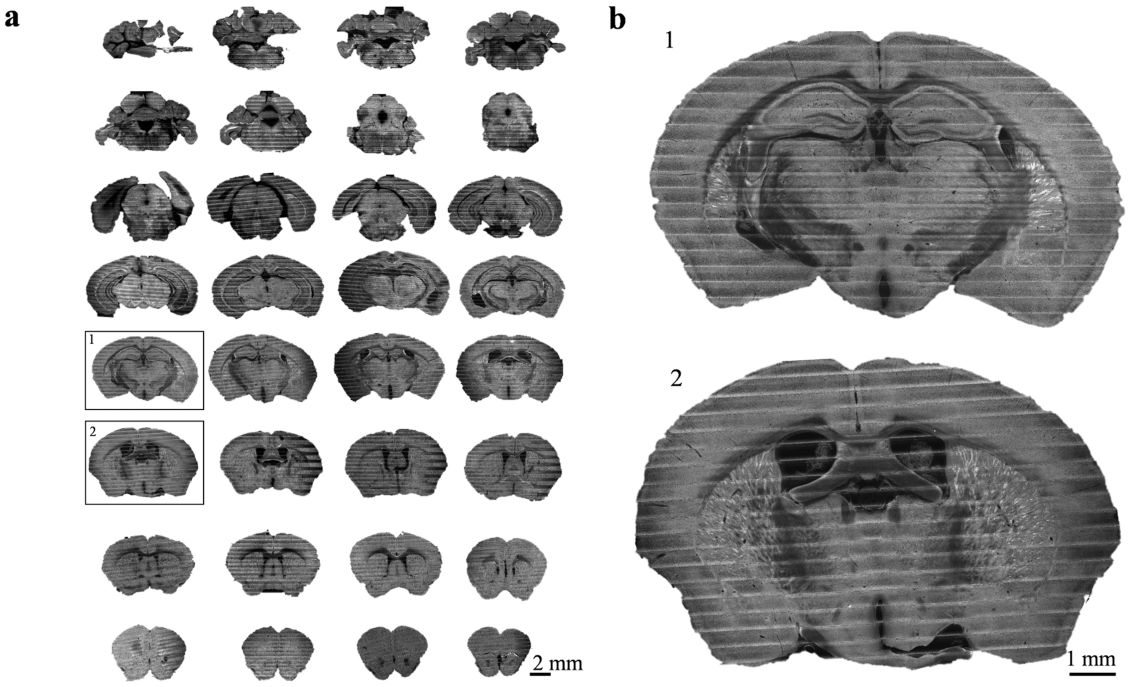

Figure 4. SRS mapping of whole mouse brain slices. (a) SRS images of 32 intact brain tissue slices. Scale bar, 2 mm. (b) Selected SRS images of two tissue slices indicated in panel (a). Scale bar, 1 mm.

for Stokes. For brain slices in Figures 3 and 4, AOD scanned 400 pixels with a step of 1 μm/pixel and a dwell time of 4 μs/pixel.

Preparation of Mouse Brain Slices for SRS Imaging. All animal experiments were carried out under ethical regulations of HUST. Adult C57 mice were selected for our experiments, and the agarose-embedded mouse brains were sliced by a vibratome to 100 μm in thickness in Figure 3 and 150 μm in Figure 4. The brain slices were further fixed overnight in 4% paraformaldehyde.

RESULTS AND DISCUSSION

AOD-Based High-Speed Large-Field Stimulated Raman Scattering Microscopy. Figure 1 shows the schematic design of AOD-based high-speed SRS imaging system (see more details in the Experimental Methods section). Two synchronized RF-driven AODs play the central role to scan the pump and Stokes lasers simultaneously. As the RF frequency is tuned from 40 to 100 MHz, the first order of AOD-diffracted beam can be scanned from 0.048 to 0.121 rad referenced to the zero-order beam (Figure 2a). The beam separation at the focus of a f = 300 mm scanning lens can reach 21.9 mm (gray shade in Figure 2a), which corresponds to ~450 μm of FOV under a 40× objective. Since the laser scanning angles are linearly proportional to laser wavelengths, we synchronized two AODs by matching and calibrating the relationship between their deflection angles and input RF frequencies for both pump and Stokes lasers to achieve perfect SRS mapping. However, for broad-band fs lasers, the wavelength-dependent angular dispersion of AOD, inducing elliptical beam distortion (Figure 2a), will be another major issue that may ruin the imaging resolution. To combat the spatial dispersion and maintain the Gaussian beams, we constructed two spectral compressor systems for both fs pump and Stokes lasers, in which the grating pair first provides negative chirping, and then in a long PM-SMF, the nonlinear effect called self-phase modulation (SPM) efficiently compresses the spectral width of the fs laser without energy loss. As shown in Figure 2b, the spectral width of a 282 mW pump laser in PM-SMF was compressed by a factor of 3.9 from 7.5 to 1.9 nm in FWHM. For a low input laser power (e.g., <1.41 mW), the spectral compressor will lose its efficacy due to low nonlinearity. Meanwhile, the spectral width of the Stokes laser at an input laser power of 286 mW can be compressed up to 5.5 times, which is about 10 cm^{-1}. As a result, the spectral narrowing of ultrafast laser pulses significantly reduced the spatial dispersion in AODs, and the laser beam shapes after AODs retained Gaussian beam profiles for flawless SRS imaging (Figure 2c).

To validate the precision of AOD-based laser scanning, we scanned the laser and directly recorded images of 450 focused laser spots by an NIR camera. Here, the input RF frequencies of the AODs were set at 46−90 MHz and 36−69 MHz for pump and Stokes lasers, respectively. Figure 2d pictures 19 pairs of equally spaced laser spots of total 450 scanning steps. The step intervals of 450 scanned points were finely tuned to equal by inputting the calibrated RF frequency for each diffraction angle. To match the steps of independently scanned pump and Stokes lasers, the spatial and temporal calibrations or alignments of AOD scanning in micron and microsecond resolution are necessary. Compared to the galvanometers, inertia-free AODs can instantly respond to RF changes and are more versatile and accurate for timing the laser pulse and positioning the laser beams during high-speed SRS imaging.

High-Speed Chemical Mapping of Intact Mouse Brain Tissues. To validate the SRS imaging speed, we perform C−H (lipids and proteins)-specific molecular mapping of an intact mouse brain slice sectioned to 100 μm in thickness. To balance the high speed and high sensitivity, a dwell time of imaging was set to 4 μs for each pixel and the AODs scanned 400 steps with an ~1 μm interval in about 1.8 ms for line scan. Due to low diffraction efficiency at both sides of AOD deflection range, we selected central 400 scanning steps for tissue imaging. Thus, a 400 μm wide and 10 mm long tissue stripe can be imaged in 20 s

https://doi.org/10.1021/acs.jpcb.2c09114
J. Phys. Chem. B 2023, 127, 4229−4234

by SRS microscope equipped with AOD scanning and motorized stage. For an intact brain slice, typically covering 12 × 8 mm^2 in area (Figure 3a), it only took about 8 min to complete high-quality SRS mapping with a spatial resolution of ~1 μm. In such resolution and scale, the complete distributions of cerebral cortex, white matter, hippocampus, and other brain structures can be visualized with great detail. We are able to observe the neurons and axons distributed across different brain regions. In Figure 3b,c, zoom-in images clearly present the fiber bundles with a strong SRS signal in different regions.

Since the SRS imaging speed has been substantially improved, we further imaged 32 consecutive intact mouse brain slices evenly sectioned from one mouse brain (Figure 4). Theoretically, it will take roughly 300 min or 5 h to perform a high-resolution SRS imaging of 32 intact brain tissue slices. However, to replace the old sample with a new slice under the objective, we spent more than 10 min each time. Also, much more extra time was taken in manual adjustment of objective focusing and searching for a new start point for imaging. Eventually, we spent about 12 h to complete SRS imaging of 32 tissue slices. An automated system will significantly save the above-mentioned auxiliary time and enable a more delicate three-dimensional (3D) organ imaging by SRS.

CONCLUSIONS

In summary, by applying inertial-free AOD scanning, we significantly improved the molecular imaging speed of large intact tissues, which was a long-standing obstacle limiting the conventional SRS microscope due to mechanical inertia of the galvanometer scanner. The laser beam distortion induced by spatial dispersion in AOD was compensated by spectral compressors converting fs lasers to ps lasers. We demonstrated high-speed high-resolution SRS imaging of intact mouse brain tissue in 8 min, and 32 tissue slices from one whole mouse brain in 12 h. In the future, the inertial-free AOD scanning-based SRS microscopy could be significantly improved and has no doubt to surpass the current imaging speed. As long as the SRS sensitivity is ensured, the dwell time can be as short as 100 ns. In theory, the total time to image a 12 × 8 mm^2 tissue will only take 10−20 s. Moreover, a low-magnification objective lens, such as a 1.05 NA, 25× objective (XLPLN25XWMP2), can double the FOV and thus enable ultimate imaging speed and tissue size. With finer tissue sectioning and system upgrades, this method is expected to examine large clinical tissues for fast bedside pathology in minutes.

ASSOCIATED CONTENT

Supporting Information

The Supporting Information is available free of charge at https://pubs.acs.org/doi/10.1021/acs.jpcb.2c09114.

Measurements of spectral widths and pulse widths after spectral compressors (PDF)

AUTHOR INFORMATION

Corresponding Authors

Xiaocong Yuan − *Research Center for Humanoid Sensing, Zhejiang Laboratory, Hangzhou 311100 Zhejiang, China;* orcid.org/0000-0003-2605-9003; Email: xcyuan@zhejianglab.com

Ping Wang − *Britton Chance Center and MoE Key Laboratory for Biomedical Photonics, Advanced Biomedical Imaging Facility, Wuhan National Laboratory for Optoelectronics-Huazhong University of Science and Technology, Wuhan 430074 Hubei, China; Optics Valley Laboratory, Wuhan 430074 Hubei, China; Huaiyin Institute of Technology, Huai'an 223001 Jiangsu, China; Changping Laboratory, Beijing 102206, China;* orcid.org/0000-0002-5168-6829; Email: p_wang@hust.edu.cn

Authors

Shuai Yan − *Britton Chance Center and MoE Key Laboratory for Biomedical Photonics, Advanced Biomedical Imaging Facility, Wuhan National Laboratory for Optoelectronics-Huazhong University of Science and Technology, Wuhan 430074 Hubei, China; Changping Laboratory, Beijing 102206, China;* orcid.org/0000-0002-9083-7749

Yiran Li − *Britton Chance Center and MoE Key Laboratory for Biomedical Photonics, Advanced Biomedical Imaging Facility, Wuhan National Laboratory for Optoelectronics-Huazhong University of Science and Technology, Wuhan 430074 Hubei, China*

Zhiliang Huang − *Britton Chance Center and MoE Key Laboratory for Biomedical Photonics, Advanced Biomedical Imaging Facility, Wuhan National Laboratory for Optoelectronics-Huazhong University of Science and Technology, Wuhan 430074 Hubei, China*

Complete contact information is available at: https://pubs.acs.org/10.1021/acs.jpcb.2c09114

Author Contributions

S.Y. and Y.L. contributed equally. S.Y. carried out the construction of the high-speed stimulated Raman scattering microscope. S.Y., Y.L., and Z.H. performed experiments. S.Y., Y.L., and P.W. analyzed the data. S.Y. and Z.H. prepared the biological samples. S.Y., Y.L., and P.W. wrote the manuscript with inputs from all authors. P.W., S.Y., and X.Y. conceived the concept. P.W. supervised the project.

Notes

The authors declare no competing financial interest.

ACKNOWLEDGMENTS

P.W. acknowledges the support from the National Natural Science Foundation of China (62075076), the Innovation Project of Optics Valley Laboratory (OVL2021BG010), and the Innovation Fund of the Wuhan National Laboratory for Optoelectronics. S.Y. acknowledges the support from China Postdoctoral Science Foundation (2021M701322) and the funding for Postdoctoral Innovation Research Post in Hubei Province. X.Y. acknowledges the support from the Key Research Project of Zhejiang Lab (K2022MG0AC05).

REFERENCES

(1) Campagnola, P. J.; Millard, A. C.; Terasaki, M.; Hoppe, P. E.; Malone, C. J.; Mohler, W. A. Three-Dimensional High-Resolution Second-Harmonic Generation Imaging of Endogenous Structural Proteins in Biological Tissues. *Biophys. J.* **2002**, *82*, 493−508.

(2) Tsai, M. R.; Cheng, Y. H.; Chen, J. S.; Sheen, Y. S.; Liao, Y. H.; Sun, C. K. Differential Diagnosis of Nonmelanoma Pigmented Skin Lesions Based on Harmonic Generation Microscopy. *J. Biomed. Opt.* **2014**, *19*, 036001.

(3) Li, Y.; Shen, B.; Zou, G.; Hu, R.; Pan, Y.; Qu, J.; Liu, L. Super-Multiplex Nonlinear Optical Imaging Unscrambles the Statistical Complexity of Cancer Subtypes and Tumor Microenvironment. *Adv. Sci.* **2022**, *9*, No. 2104379.

(4) Wang, K.; Xu, C. Tunable High-Energy Soliton Pulse Generation from a Large-Mode-Area Fiber and Its Application to Third Harmonic Generation Microscopy. *Appl. Phys. Lett.* **2011**, *99*, No. 071112.
(5) Puliafito, C. A.; Hee, M. R.; Lin, C. P.; Reichel, E.; Schuman, J. S.; Duker, J. S.; Izatt, J. A.; Swanson, E. A.; Fujimoto, J. G. Imaging of Macular Diseases with Optical Coherence Tomography. *Ophthalmology* **1995**, *102*, 217−229.
(6) Potma, E. O.; Knez, D.; Chen, Y.; Davydova, Y.; Durkin, A.; Fast, A.; Balu, M.; Norton-Baker, B.; Martin, R. W.; Baldacchini, T.; Fishman, D. A. Rapid Chemically Selective 3d Imaging in the Mid-Infrared. *Optica* **2021**, *8*, 995−1002.
(7) Wang, L. V.; Yao, J. A Practical Guide to Photoacoustic Tomography in the Life Sciences. *Nat. Methods* **2016**, *13*, 627−638.
(8) Zhang, D.; Li, C.; Zhang, C.; Slipchenko, M. N.; Eakins, G.; Cheng, J. X. Depth-Resolved Mid-Infrared Photothermal Imaging of Living Cells and Organisms with Submicrometer Spatial Resolution. *Sci. Adv.* **2016**, *2*, No. e1600521.
(9) Kumamoto, Y.; Harada, Y.; Takamatsu, T.; Tanaka, H. Label-Free Molecular Imaging and Analysis by Raman Spectroscopy. *Acta Histochem. Cytochem.* **2018**, *51*, 101−110.
(10) Freudiger, C. W.; Min, W.; Saar, B. G.; Lu, S.; Holtom, G. R.; He, C.; Tsai, J. C.; Kang, J. X.; Xie, X. S. Label-Free Biomedical Imaging with High Sensitivity by Stimulated Raman Scattering Microscopy. *Science* **2008**, *322*, 1857−1861.
(11) Cheng, J.-X.; Xie, X. S. *Coherent Raman Scattering Microscopy*; CRC Press, 2012.
(12) Saar, B. G.; Freudiger, C. W.; Reichman, J.; Stanley, C. M.; Holtom, G. R.; Xie, X. S. Video-Rate Molecular Imaging in Vivo with Stimulated Raman Scattering. *Science* **2010**, *330*, 1368−1370.
(13) Figueroa, B.; Nguyen, T.; Sotthivirat, S.; Xu, W.; Rhodes, T.; Lamm, M. S.; Smith, R. L.; John, C. T.; Su, Y.; Fu, D. Detecting and Quantifying Microscale Chemical Reactions in Pharmaceutical Tablets by Stimulated Raman Scattering Microscopy. *Anal. Chem.* **2019**, *91*, 6894−6901.
(14) Li, H.; Cheng, Y.; Tang, H.; Bi, Y.; Chen, Y.; Yang, G.; Guo, S.; Tian, S.; Liao, J.; Lv, X.; et al. Imaging Chemical Kinetics of Radical Polymerization with an Ultrafast Coherent Raman Microscope. *Adv. Sci.* **2020**, *7*, No. 1903644.
(15) Nitta, N.; Iino, T.; Isozaki, A.; Yamagishi, M.; Kitahama, Y.; Sakuma, S.; Suzuki, Y.; Tezuka, H.; Oikawa, M.; Arai, F.; et al. Raman Image-Activated Cell Sorting. *Nat. Commun.* **2020**, *11*, No. 3452.
(16) Bi, Y.; Yang, C.; Chen, Y.; Yan, S.; Yang, G.; Wu, Y.; Zhang, G.; Wang, P. Near-Resonance Enhanced Label-Free Stimulated Raman Scattering Microscopy with Spatial Resolution near 130 Nm. *Light: Sci. Appl.* **2018**, *7*, 81.
(17) Yue, S.; Li, J.; Lee, S. Y.; Lee, H. J.; Shao, T.; Song, B.; Cheng, L.; Masterson, T. A.; Liu, X.; Ratliff, T. L.; Cheng, J. X. Cholesteryl Ester Accumulation Induced by Pten Loss and Pi3k/Akt Activation Underlies Human Prostate Cancer Aggressiveness. *Cell Metab.* **2014**, *19*, 393−406.
(18) Zhang, L.; Shi, L.; Shen, Y.; Miao, Y.; Wei, M.; Qian, N.; Liu, Y.; Min, W. Spectral Tracing of Deuterium for Imaging Glucose Metabolism. *Nat. Biomed. Eng.* **2019**, *3*, 402−413.
(19) Schie, I. W.; Krafft, C.; Popp, J. Applications of Coherent Raman Scattering Microscopies to Clinical and Biological Studies. *Analyst* **2015**, *140*, 3897−3909.
(20) Ji, M.; Orringer, D. A.; Freudiger, C. W.; Ramkissoon, S.; Liu, X.; Lau, D.; Golby, A. J.; Norton, I.; Hayashi, M.; Agar, N. Y.; et al. Rapid, Label-Free Detection of Brain Tumors with Stimulated Raman Scattering Microscopy. *Sci. Transl. Med.* **2013**, *5*, No. 201ra119.
(21) Camp, C. H., Jr.; Lee, Y. J.; Heddleston, J. M.; Hartshorn, C. M.; Hight Walker, A. R.; Rich, J. N.; Lathia, J. D.; Cicerone, M. T. High-Speed Coherent Raman Fingerprint Imaging of Biological Tissues. *Nat. Photonics* **2014**, *8*, 627−634.
(22) Ji, M.; Lewis, S.; Camelo-Piragua, S.; Ramkissoon, S. H.; Snuderl, M.; Venneti, S.; Fisher-Hubbard, A.; Garrard, M.; Fu, D.; Wang, A. C.; et al. Detection of Human Brain Tumor Infiltration with Quantitative Stimulated Raman Scattering Microscopy. *Sci. Transl. Med.* **2015**, *7*, No. 309ra163.
(23) Lu, F. K.; Calligaris, D.; Olubiyi, O. I.; Norton, I.; Yang, W.; Santagata, S.; Xie, X. S.; Golby, A. J.; Agar, N. Y. Label-Free Neurosurgical Pathology with Stimulated Raman Imaging. *Cancer Res.* **2016**, *76*, 3451−3462.
(24) Galli, R.; Uckermann, O.; Temme, A.; Leipnitz, E.; Meinhardt, M.; Koch, E.; Schackert, G.; Steiner, G.; Kirsch, M. Assessing the Efficacy of Coherent Anti-Stokes Raman Scattering Microscopy for the Detection of Infiltrating Glioblastoma in Fresh Brain Samples. *J. Biophotonics* **2017**, *10*, 404−414.
(25) Pekmezci, M.; Morshed, R. A.; Chunduru, P.; Pandian, B.; Young, J.; Villanueva-Meyer, J. E.; Tihan, T.; Sloan, E. A.; Aghi, M. K.; Molinaro, A. M.; et al. Detection of Glioma Infiltration at the Tumor Margin Using Quantitative Stimulated Raman Scattering Histology. *Sci. Rep.* **2021**, *11*, No. 12162.
(26) He, R.; Xu, Y.; Zhang, L.; Ma, S.; Wang, X.; Ye, D.; Ji, M. Dual-Phase Stimulated Raman Scattering Microscopy for Real-Time Two-Color Imaging. *Optica* **2017**, *4*, 44−47.
(27) Zhang, B.; Sun, M.; Yang, Y.; Chen, L.; Zou, X.; Yang, T.; Hua, Y.; Ji, M. Rapid, Large-Scale Stimulated Raman Histology with Strip Mosaicing and Dual-Phase Detection. *Biomed. Opt. Express* **2018**, *9*, 2604−2613.
(28) Lin, H.; Lee, H. J.; Tague, N.; Lugagne, J. B.; Zong, C.; Deng, F.; Shin, J.; Tian, L.; Wong, W.; Dunlop, M. J.; Cheng, J. X. Microsecond Fingerprint Stimulated Raman Spectroscopic Imaging by Ultrafast Tuning and Spatial-Spectral Learning. *Nat. Commun.* **2021**, *12*, No. 3052.
(29) Ozeki, Y.; Umemura, W.; Otsuka, Y.; Satoh, S.; Hashimoto, H.; Sumimura, K.; Nishizawa, N.; Fukui, K.; Itoh, K. High-Speed Molecular Spectral Imaging of Tissue with Stimulated Raman Scattering. *Nat. Photonics* **2012**, *6*, 845−851.
(30) Xu, Z.; Pan, Y.; Chen, N.; Zeng, S.; Liu, L.; Gao, R.; Zhang, J.; Fang, C.; Song, L.; Liu, C. Visualizing Tumor Angiogenesis and Boundary with Polygon-Scanning Multiscale Photoacoustic Microscopy. *Photoacoustics* **2022**, *26*, No. 100342.
(31) Zheng, T.; Yang, Z.; Li, A.; Lv, X.; Zhou, Z.; Wang, X.; Qi, X.; Li, S.; Luo, Q.; Gong, H.; Zeng, S. Visualization of Brain Circuits Using Two-Photon Fluorescence Micro-Optical Sectioning Tomography. *Opt. Express* **2013**, *21*, 9839−9850.

https://doi.org/10.1021/acs.jpcb.2c09114
J. Phys. Chem. B 2023, 127, 4229−4234